JURNAL SAINS MATERI INDONESIA (JUSAMI)
ISSN: 1411-1098 (print), 2614-087X (online)
VOL. 27, ISSUE 2, 2026
DOI: https://doi.org/10.55981/jsmi.2026.11718

ORIGINAL ARTICLE

High Temperature Corrosion On Inconel and Carbon Steel Filler of Weldment in Liquid Pb at 800 ˚C

A.P.A. Mustari[1,*], H. Wafda[2] and P.M. Adhi[3]

[1]Faculty of Mathematics and Natural Sciences, Institut Teknologi Bandung, Jl. Ganesha 10, Bandung 40132, Indonesia
[2]Research Center for Nuclear Reactor Technology, Research Organization for Nuclear Energy, National Research and Innovation Agency, South Tangerang 15310, Indonesia
[3]Applied Master Program in Manufacturing Technology Engineering, Politeknik Negeri Jakarta, Prof. G.A. Siwabessy Street, UI Campus, Depok 16425, Indonesia

ABSTRACT – This study evaluates the corrosion behavior of SS316 material welded using Inconel and 70S fillers in a static liquid lead (Pb) environment saturated with oxygen at 800 °C for 36 hours, simulating accident conditions in a lead-cooled fast reactor (LFR). Welding was carried out using laser welding (Inconel filler) and metal inert gas (MIG) (70S filler) methods, representing structural joints in the reactor. The results of scanning electron microscope (SEM) and energy dispersive X-ray (EDX) analysis showed the formation of a spinel-type oxide layer (Fe-Cr-O) in both weld areas, with the laser welding sample showing deeper Pb penetration due to the porosity of the oxide layer. In contrast, in MIG welding, the oxide layer was denser with limited Pb penetration at the spinel-matrix interface. The base metal (BM) only formed a thin layer without significant oxide, but showed lower Pb penetration. These results provide critical insights into filler metal performance under extreme conditions, supporting material selection and weld design strategies for enhanced safety and longevity in next-generation lead-cooled fast reactors.

ARTICLE HISTORY
Received: 13 Jun 2025
Revised: 18 Jul 2025
Accepted: 11 August 2025

KEYWORDS
Lead-cooled fast reactor (LFR)
Welded SS316
Inconel and 70S filler
High-temperature corrosion
Oxide scale

INTRODUCTION

A lead-cooled fast reactor (LFR) is one of the proposed reactors in Generation IV reactors, which is intended to generate high efficiency and inherent safety due to the use of Pb as a coolant. The advantage of LFR is its thermal stability at high temperatures and its fast neutron spectrum, which will transmute minor actinides [1]–[3]. In addition, passive safety systems, such as natural convection, are capable of removing residual heat without requiring operator intervention. However, a major challenge is its corrosion behavior on structural materials, which requires maintaining a certain oxygen concentration to form a protective oxide layer [4], [5]. Such corrosion can compromise the integrity of reactor components.

Welding plays a crucial role in the power plant system, serving to connect structural components, pipes, and other vital components within the system. However, welded joints are often vulnerable points due to microstructural changes, weld defects, and residual stresses induced during the welding process. Non-uniform microstructures in the heat-affected zone (HAZ) can trigger crack initiation due to creep or fatigue, as well as amplify residual stresses that facilitate stress corrosion cracking (SCC) [6]–[8]. Welding defects, such as porosity, inclusions, and hot cracks, also increase the risk of mechanical damage and local corrosion [9]–[11]. This condition is even more critical in extreme operations such as molten metal environments (e.g., Pb), where the combination of high temperatures and aggressive media can accelerate weld joint failure. Therefore, standardization of weld quality, reduction of residual stress techniques (e.g., post weld heat treatment, PWHT, or shot peening), and the use of fillers and corrosion-resistant materials are essential to ensure the long-term reliability of the generating system. Fusion welding techniques with different thermal characteristics, such as high-precision low-heat-input processes and conventional high-heat-input methods, can significantly influence the corrosion behavior of structural joints in liquid metal environments. Comparing representative methods like laser welding and metal inert gas (MIG) welding allows insight into how variations in heat input, microstructure, and filler interactions affect corrosion resistance at high temperatures.

*CORRESPONDING AUTHOR | A. P. A. Mustari | ✉ pramutadi@itb.ac.id

In the welding process, fillers are used to ensure the integrity of the joint and improve mechanical properties, such as tensile strength and fatigue resistance. Commonly used filler types include stainless steel, nickel-based alloys such as Inconel, and carbon steel, depending on the application and operating environment. However, studies on the corrosion behavior of fillers in liquid metal environments, especially lead (Pb) or lead-bismuth eutectic (LBE) at high temperatures, are still very limited. For example, research by Charalampopoulou et al. [12] and subsequent studies on ferritic-martensitic (FM) steels such as HCM12A show that although there is corrosion data for basic materials, data for fillers is very limited [5], [13]. Several studies of nickel-based fillers such as Inconel 625 have tested corrosion under molten salt and high-temperature conditions [14], [15], but implementation in molten lead environments are still rare. This condition indicates a significant knowledge gap. Therefore, systematic research on filler corrosion in a liquid Pb environment is needed to support welding reliability in lead-cooled fast reactors (LFRs).

The 2011 Fukushima Daiichi nuclear accident was caused by a strong earthquake, a subsequent tsunami, and the failure of cooling lines and backup power systems (station blackout, SBO), which resulted in damage to the reactor core and posed a threat of a massive release of radionuclides [16]. This incident offers a valuable lesson in modern reactor design, highlighting the importance of examining beyond-design-basis events to enhance passive safety features, corrosion mitigation, and crisis management. Extreme conditions, such as high temperatures, exposure to corrosive vapors, and corrosion from water-metal interactions in emergencies, can accelerate material deterioration, particularly in weld areas susceptible to SCC. Therefore, there is an urgent need for comprehensive research simulating accident conditions—including temperature, pressure, radiation, and corrosive media—to validate the durability of weld joint materials under extreme conditions, improving the reliability and safety of future nuclear reactors.

The purpose of this study is to investigate the corrosion behavior of welded joints using carbon steel and nickel-based alloy fillers, with laser and MIG welding techniques employed, respectively. SS316 was selected as the parent material due to its favorable combination of corrosion resistance, mechanical properties, and widespread application in nuclear-grade piping and structural components, including potential use in LFR systems under controlled oxygen conditions. Tests were conducted in a lead melt environment at high temperatures (800 °C) for 36 hours to simulate extreme nuclear accident conditions. To simulate beyond-design-basis accident (BDBA) conditions in LFRs, corrosion tests were conducted at 800 °C under static conditions for 36 hours. Although LFRs employ natural circulation to maintain core cooling during SBO events, failure of ultimate heat sinks or limitations in decay heat removal systems may still result in elevated core temperatures. Therefore, testing at this elevated temperature provides conservative and safety-relevant data for assessing the structural integrity of welded materials. This research aims to understand the degradation mechanisms occurring at the weld zones, particularly in the filler materials, and to provide valuable data for improving the corrosion resistance of structural joints in the development of Generation IV nuclear reactors.

EXPERIMENTAL METHOD

Materials

The material used in this study is stainless steel 316 (SS316), a commonly used austenitic stainless steel known for its excellent corrosion resistance, high-temperature strength, and good weldability (see Table 1). The samples were rectangular plates with line-shaped welds, representing practical geometries in structural applications (Figure 1). Each welded plate had dimensions of 20 mm × 15 mm × 3 mm. To evaluate the impact of welding methods on corrosion performance in high-temperature lead environments, two welding techniques were applied: laser welding and metal inert gas (MIG) welding.

Laser welding was performed using Inconel filler wire (ERNiCrMo-3, AWS A5.14). The main welding parameters included a scan speed of 400 mm/s, a scan width of 2 mm, a peak power of 600 W, a duty cycle of 100%, and a frequency of 5000 Hz. This method is known for its precision and minimal heat-affected zone, resulting in a fine microstructure [8]. MIG welding was performed using 70S filler (AWS A5.18)[17]. The welding process used a current of 80 A and a voltage of 24.4 V. MIG welding is widely used due to its cost-effectiveness, but it produces a broader heat-affected zone and coarser grain structures compared to laser welding [9].

Table 1. Chemical composition of SS316 and filler (wt%)

	C	Mn	Si	P	S	Cr	Mo	Ni	N	Fe	Nb	Ti	Cu
SS316	≤ 0.08	≤ 2.00	≤ 0.75	≤ 0.045	≤ 0.03	16.0–18.0	2.00–3.00	10.0–14.0	≤ 0.10	Bal	-	-	-
70S [18]	0.06–0.15	1.4–1.85	0.8–1.15	<0.025	<0.035	-	-	-	-	Bal	-	-	<0.5
Inconel [14]	-	-	-	-	-	21.52	9.02	63.03	-	2.57	3.65	0.21	-

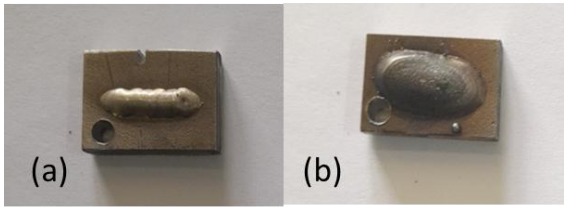

Figure 1. Samples of SS316 with laser welding (left) and MIG welding (right)

Procedure

The static corrosion testing setup was designed to evaluate the high-temperature corrosion behavior of SS316 in a liquid lead (Pb) environment under saturated oxygen conditions (see Figure 2). Commercial-grade lead with approximately 99% purity was used, which is sufficient to minimize interference from minor alloying elements in the corrosion process. The apparatus consisted of a corrosion pot made from alumina ceramic, selected for its excellent resistance to high temperatures and chemical stability. To monitor and maintain the desired temperature, a thermocouple was employed and insulated with a ceramic tube to prevent contamination and ensure accurate readings. The setup included a temperature control system to precisely regulate the test temperature, ensuring stable conditions throughout the experiment. During the corrosion test, all samples were fully immersed in molten lead, ensuring that the entire welded zone and surrounding base metal were uniformly exposed to the high-temperature corrosive environment.

Saturated oxygen conditions were achieved by creating a small opening in the autoclave during the test. This allowed direct contact between the liquid lead and ambient air, facilitating a consistent supply of oxygen. This approach ensured that the lead environment remained saturated with oxygen throughout the testing period.

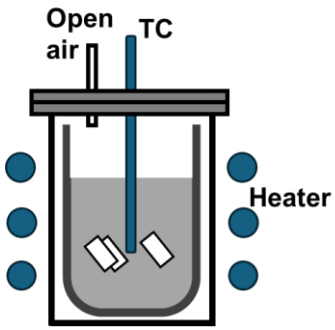

Figure 2. Schematic diagram of static test apparatus

The corrosion tests were conducted in static conditions for 36 hours at 800 °C, with saturated oxygen conditions maintained by creating a small opening in the autoclave, allowing direct contact with ambient air. Approximately 1 L of molten lead was used in the test, ensuring that all samples were immersed. The oxygen concentration (Co) in liquid lead was calculated using the equation (1) [19]:

Lead (for $300^{\circ}C < T < 1100^{\circ}C$)

$$log C^{\circ}_{O(wt.\%)} = 3.23 - \frac{5043}{T_{(K)}} \quad (1)$$

where T(K) is the temperature in Kelvin. This provided an estimate of the dissolved oxygen concentration in lead at both temperatures, ensuring consistency across experiments. The oxygen concentration (Co) was calculated to be 1.86E-01 mass% at ~800˚C.

After the corrosion test, the sample cleaning process was performed using an acid solution composed of ethanol, 30% hydrogen peroxide, and 99% acetic acid in a 1:1:1 volume ratio, followed by ultrasonic rinsing with ethanol to remove any remaining residues. The samples are then mounted in resin. The observation was conducted using scanning electron microscopy (SEM) and energy dispersive X-ray spectroscopy (EDX). Map and line analysis was conducted.

RESULT

Figure 3 presents scanning electron microscopy (SEM) micrographs of cross-sectional surfaces from laser-welded (left) and metal inert gas (MIG)-welded (right) regions after exposure to static lead (Pb) at 800 °C for 36 hours. Both welding methods produced thick and homogeneous oxide layers, indicating substantial oxidation under these high-temperature conditions. However, differences in the mechanical integrity of the oxide layers are evident.

The laser-welded sample exhibits cracks within the oxide layer, accompanied by noticeable delamination in certain regions. These features suggest that the oxide layer on the laser-welded surface is less mechanically stable, potentially due to higher residual stresses or weaker bonding with the substrate. Such imperfections could expose the underlying metal to further corrosion, reducing the protective function of the oxide layer.

The MIG-welded sample demonstrates a generally intact oxide layer with no significant delamination and only minor cracks observed in certain areas, similar to the laser-welded sample. This suggests acceptable mechanical stability and adhesion to the substrate, which may help maintain corrosion resistance during exposure to liquid lead at elevated temperatures. While both welding methods show some degree of cracking, the MIG-welded sample tends to form a denser and more protective oxide layer. This underscores the influence of filler material and welding technique on the structural integrity of the oxide scale in high-temperature lead environments.

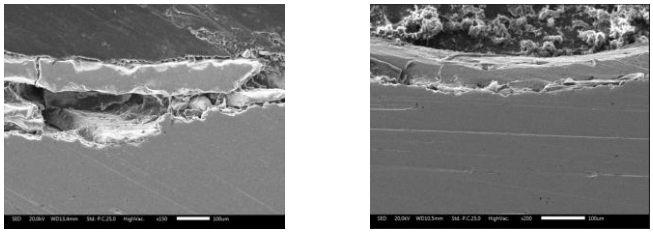

Figure 3. SEM images of the cross-sections of SS316 welded by laser (left) and MIG (right) after exposure in static oxygen-saturated liquid Pb for 36 h at 800 °C

Figure 4 shows the cross-sectional elemental mapping of stainless steel 316 (SS316) samples welded using Inconel filler after exposure to a static Pb environment with oxygen saturation at ~800 °C for 36 hours. A relatively uniform oxide scale is seen on the surface, indicating a stable oxidation reaction. Based on the distribution of iron (Fe), chromium (Cr), and oxygen (O) elements, spinel is likely to form as a result of the reaction between the three elements. In addition, nickel (Ni) elements were also detected in the scale, indicating that Ni from the Inconel filler participated in the oxide formation or experienced partial dissolution. Pb is seen filling the pores in the oxide scale, indicating that although the oxide layer is formed, there are still entry paths for Pb into the oxide structure due to porosity or microcracks. Interestingly, although the test was carried out at a high temperature (~800 °C), the relatively short duration (36 hours) allows the dissolution process of the metal into Pb to be more dominant than the growth of a compact and protective oxide layer.

Figure 5 shows the cross-sectional elemental mapping of SS316 samples welded using 70S filler (MIG welding) after being exposed to a static oxygen-saturated Pb environment at ~800 °C for 36 hours. It can be seen that the spinel layer is formed relatively uniformly along the surface without any indication of significant delamination or damage to the layer. The distribution of Pb elements also shows no significant penetration into the oxide layer or the substrate. This indicates that the spinel formed functions quite effectively as a protective layer against liquid metal intrusion. The existence of this more stable protective layer indicates that, under these test conditions, the oxidation reaction dominates over the dissolution process of metal elements into liquid Pb. This is possible because the characteristics of the oxide formed from MIG welding with carbon filler are denser and can withstand Pb diffusion more effectively in a relatively short exposure time.

Figure 6 shows the cross-sectional elemental mapping of SS316 base metal (BM) after exposure to a static oxygen-saturated Pb environment at ~800 °C for 36 hours. It can be seen that the formed oxide layer (scale) is very thin and non-uniform, indicating that the oxidation rate on the BM surface is relatively low. Based on the distribution of Fe, Cr, and Ni elements, all three have dissolved into Pb, indicating that the dissolution process has occurred, although to a limited extent. Pb elements appear to fill the surface area of the layer. However, the oxygen distribution does not show significant penetration into the layer, indicating that the protective oxide layer is not formed effectively. However, compared to the welded samples (with Inconel and 70S fillers), corrosion on SS316 base metal appears more minimal, with lower Pb penetration and surface degradation. This indicates that under these conditions, SS316 BM exhibits relatively better corrosion resistance.

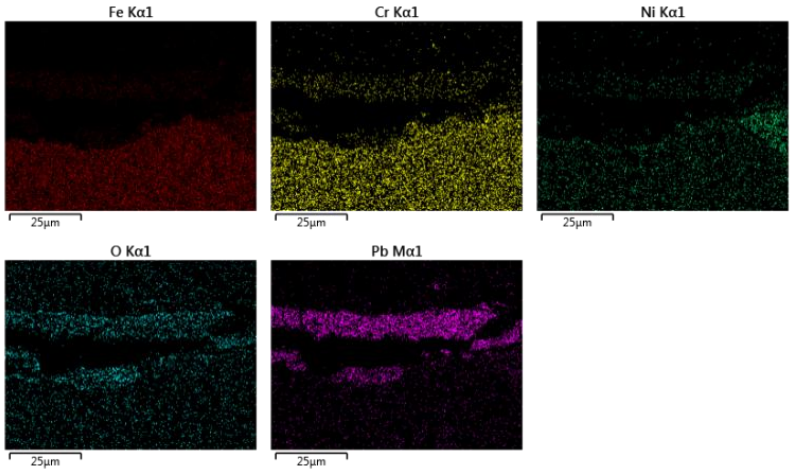

Figure 3. Cross-sectional elemental mapping of laser-welded SS316 after exposure at ~800 °C for 36 h in static Pb

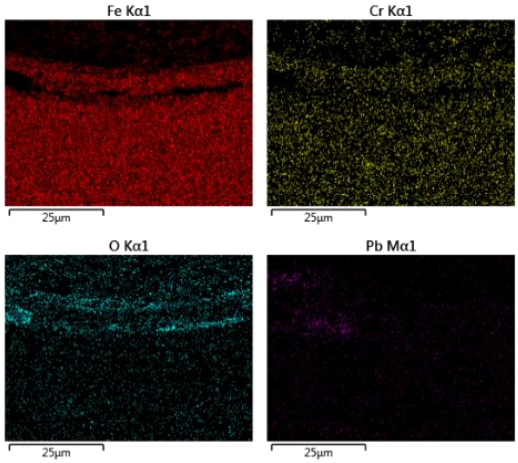

Figure 4. Cross-sectional elemental mapping of MIG-welded SS316 after exposure at 800 °C for 36 h in static Pb

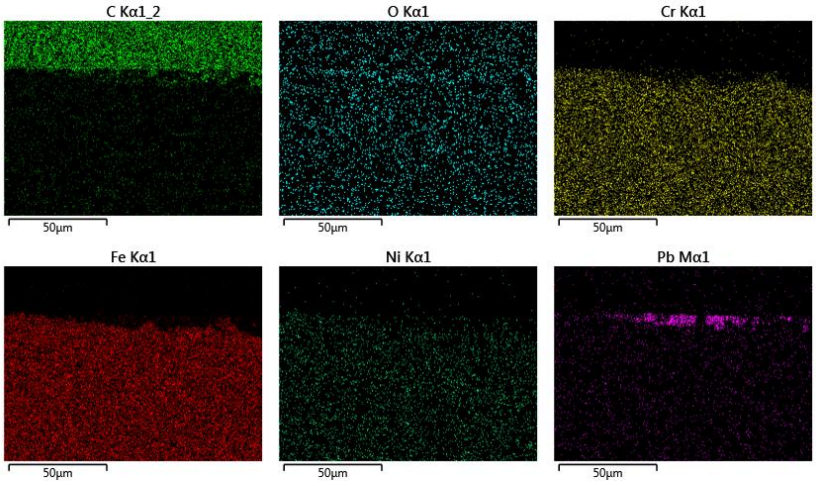

Figure 6. Cross-sectional elemental mapping of SS316 BM after exposure at 800 °C for 36 h in static Pb

In Figure 7, corresponding to the laser-welded sample, a distinct oxide scale is observed, characterized by elevated Fe, Cr, and O signals, indicating the formation of spinel-type oxides. Notably, Pb is detected throughout the scale region, confirming that lead has occupied the oxide structure. This suggests that the oxide layer formed at this high temperature is porous or contains microcracks, allowing Pb to penetrate deeply into the material. Such porosity may result from thermal stress or incomplete densification during short-term exposure.

In Figure 8, representing the MIG-welded sample, a similar enrichment of Cr and O is observed in the oxide layer, suggesting spinel formation as well. However, the amount of Pb detected is lower than that in the laser-welded sample.

Pb appears localized near the interface between the oxide and the metal matrix, indicating that its ingress may occur through localized cracking rather than the entire oxide layer, implying relatively better oxide integrity.

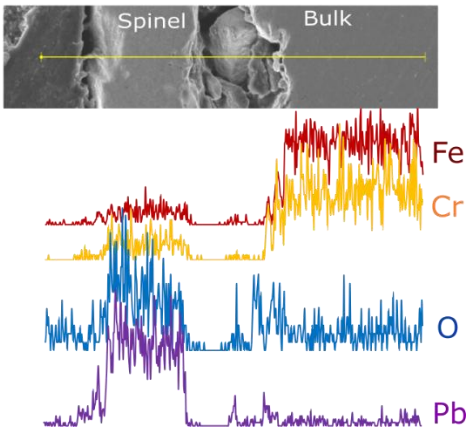

Figure 7. EDX line scan of laser-welded SS316 after exposure at ~800 °C for 36 h in static Pb

.

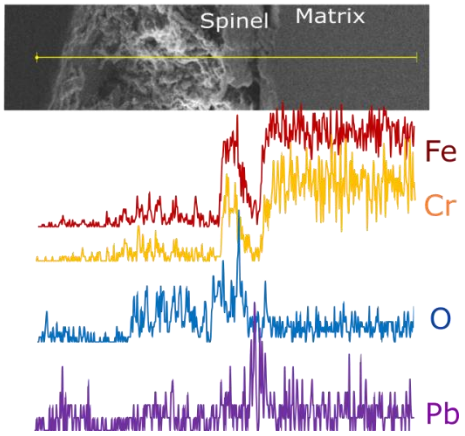

Figure 5. EDX line scan of MIG-welded SS316 after exposure at 800 °C for 36 h in static Pb

DISCUSSION

At 800 °C, the oxidation rate increases significantly, allowing the formation of an oxide layer in a short time, mainly in the form of iron-chromium-oxygen (Fe-Cr-O)-based spinel. All welded samples (laser and metal inert gas, MIG) exhibit relatively even spinel formation. In contrast, the stainless steel 316 (SS316) base metal (BM) displays only a thin layer with indications of lead (Pb) penetration and selective dissolution of elements such as Fe, Cr, and nickel (Ni). This indicates that in BM, the spinel is likely to form very thinly and not provide protection. The rate of spinel formation at high temperatures is significantly influenced by the microstructure formed during the welding process, including grain size and residual stress distribution. In addition, the chemical composition of the oxide layer is highly dependent on the type of filler (Inconel vs. 70S) used and the welding method (laser vs. MIG), as reported by Fazio et al. [20], Lambrinou et al. [21], and Olson et al. [15].

In the laser-welded sample with Inconel 625 filler, a fairly uniform spinel oxide layer was formed along the surface. However, elemental mapping revealed that Fe, Cr, and Ni were detected in areas directly associated with liquid Pb, indicating that these elements had dissolved from the weld metal into the Pb environment. In addition, Pb was also detected filling the oxide structure, indicating that the oxide scale is porous and allows penetration of the liquid metal. This condition indicates that although high temperatures (800 °C) encourage oxide formation, short exposure times (36 hours) are not enough to form a compact and protective oxide layer. As a result, the dissolution reaction is more dominant than the formation of protective oxide, which is in line with similar findings in the study of Inconel 625 corrosion in high-temperature molten salt environments [14].

In the MIG welding sample using ER70S filler, a smooth and relatively stable spinel layer was formed on the metal surface. Although there were some microcracks in the oxide layer, Pb was detected only in a limited manner at the

interface between the spinel and the matrix, indicating that the spinel layer still functions as a fairly effective barrier. This indicates that the oxidation reaction is more dominant than the dissolution of the metal into Pb. The microstructure of MIG welding tends to form coarser grains. It produces lower residual stress than laser welding, making it more resistant to thermal cracking and Pb penetration, as explained by Jiang et al. [22] and Coelho et al. [23].

Figure 9 shows the thickness of the oxide layer (scale) on the samples with laser welding using Inconel filler, MIG welding with 70S filler, and SS316 base metal (BM) after exposure to static oxygen-saturated Pb at a temperature of 800 °C for 36 hours. The highest layer thickness is found in laser welding (~90 µm), followed by MIG welding (~85 µm), while BM is only around ~50 µm. However, the layer on the BM formed has a thin selective dissolution layer, indicating better corrosion resistance compared to both types of fillers. In samples with Inconel and 70S fillers, the spinel layer is indeed formed thicker, but is more porous or shows interface cracks, making it less protective. These results are in line with the studies of Lambrinou et al. [21] and Charalampopoulou et al. [12], which show that the morphology and integrity of the oxide are greatly determined by the type of filler and the microstructure of the welding results.

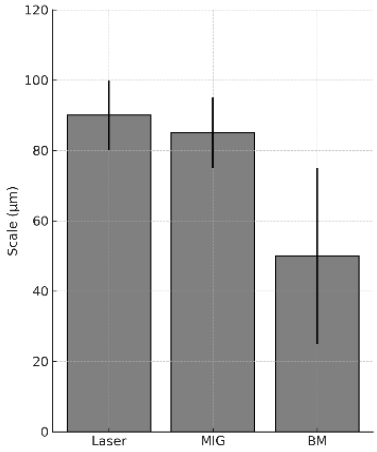

Figure 6. Scale thicknesses of laser-welded, MIG-welded, and base metal (BM) specimens after exposure at 800 °C

Figure 10 explains the corrosion behavior of SS316 from laser welding, MIG, and base metal (BM) after exposure to static Pb saturated with oxygen at a temperature of 800 °C. In laser welding with Inconel filler, selective dissolution of Fe, Cr, and Ni elements occurs into Pb, then reacts with oxygen to form an oxide layer. However, the oxide formed is porous, so Pb can still penetrate and fill the layer. In MIG welding with 70S filler (carbon steel), selective dissolution is limited to Fe and Cr, forming a denser oxide. However, cracks in the layer allow Pb penetration to the interface with the base metal. Meanwhile, in the SS316 base metal (BM), there is almost no detectable oxide layer; what is visible is the surface that experiences selective dissolution and direct penetration by Pb. This condition indicates that, despite the minimal layer, Pb penetration is more limited than in the weld area.

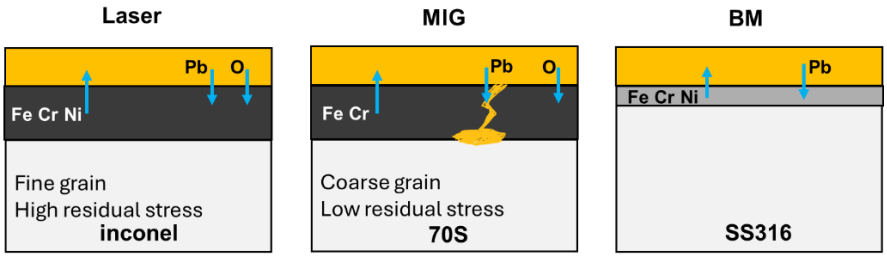

Figure 7. Corrosion behavior on welded surfaces and BM

CONCLUSION

Corrosion testing at 800 °C in static oxygen-saturated liquid lead (Pb) showed that the welded stainless steel 316 (SS316) developed iron-chromium-oxygen (Fe–Cr–O-based) oxide layers. In contrast, the base metal (BM) exhibited selective dissolution with the formation of only a very thin surface layer. Laser welding with Inconel filler resulted in a thicker but porous oxide layer, which facilitated deeper Pb penetration due to the selective dissolution of Fe, Cr, and nickel (Ni) elements. Conversely, metal inert gas (MIG) welding with 70S filler produced a denser and more protective oxide scale, although localized cracks permitted Pb ingress at the oxide–metal interface. Among the three regions, the base metal demonstrated superior corrosion resistance, characterized by minimal Pb penetration and negligible oxide

formation. These findings confirm that both filler composition and welding technique critically influence the integrity of oxide layers and the overall corrosion resistance, which are key considerations for structural material performance in lead-cooled fast reactor (LFR) environments.

ACKNOWLEDGEMENT

This research was financially supported by the Institut Teknologi Bandung (ITB) through the "Program Riset Unggulan ITB 2025" under contract number 841/IT1.B07.1/TA.00/2025.

REFERENCES

[1] L. Cinotti, C. F. Smith, H. Sekimoto, L. Mansani, M. Reale, and J. J. Sienicki. "Lead-cooled System Design and Challenges in the Frame of Generation IV International Forum." *J. Nucl. Mater.*, vol. 415, no. 3, pp. 245–253, 2011.

[2] C. Zhang, L. Chen, Y. Zhang, and S. Li. "Advancements and Development Trends in Lead-Cooled Fast Reactor Core Design." *Processes*, vol. 13, no. 6, p. 1773, 2025.

[3] MIT OpenCourseware, "Under, Over and Critical Damping 1. Response to Damping," pp. 2–7, 2011/. [Online]. Available: https://ocw.mit.edu/courses/mathematics/18-03sc-differential-equations-fall-2011/unit-ii-second-order-constant-coefficient-linear-equations/damped-harmonic-oscillators/MIT18_03SCF11_s13_2text.pdf.

[4] L. Martinelli, T. Dufrenoy, K. Jaakou, A. Rusanov, and F. Balbaud-Célérier. "High Temperature Oxidation of Fe-9Cr-1Mo Steel in Stagnant Liquid Lead-Bismuth at Several Temperatures and for Different Lead Contents in the Liquid Alloy." *J. Nucl. Mater.*, vol. 376, no. 3, pp. 282–288, 2008.

[5] A. P. A. Mustari and M. Takahashi. "Study on Corrosion of Welded Steel for LBE-cooled Fast Reactors." *Progress in Nuclear Energy*, vol. 53, no. 7, pp. 1073–1077, 2011.

[6] Q. Peng, H. Xue, J. Hou, K. Sakaguchi, Y. Takeda, J. Kuniya, and T. Shoji. "Role of Water Chemistry and Microstructure in Stress Corrosion Cracking in the Fusion Boundary Region of An Alloy 182-A533B Low Alloy Steel Dissimilar Weld Joint in High Temperature Water." *Corros. Sci.*, vol. 53, no. 12, pp. 4309–4317, 2011.

[7] P. B. Srinivasan, S. Riekehr, C. Blawert, W. Dietzel, and M. Koçak. "Slow Strain Rate Stress Corrosion Cracking Behaviour of As-Welded and Plasma Electrolytic Oxidation Treated AZ31HP Magnesium Alloy Autogenous Laser Beam Weldment." *Mater. Sci. Eng. A*, vol. 517, no. 1–2, pp. 197–203, 2009.

[8] Z. Lu, T. Shoji, Y. Takeda, Y. Ito, A. Kai, and N. Tsuchiya. "Effects of Loading Mode and Water Chemistry on Stress Corrosion Crack Growth Behavior of 316L HAZ and Weld Metal Materials in High Temperature Pure Water." *Corros. Sci.*, vol. 50, no. 3, pp. 625–638, 2008.

[9] S. Edition, *Metallurgy Second Edition Welding Metallurgy*, vol. 822, no. 1–3, p. 466, 2003.

[10] X. Yang, Q. Guo, S. Tang, L. Zhang, X. Chen, and X. Shi. "Welding Numerical Simulation Analysis of AP 1000 Insert Plate and Penetration Sleeves Based on ABAQUS." *J. Phys. Conf. Ser.*, vol. 2383, no. 1, 2022.

[11] B. Bezensek and J. W. Hancock. "The Toughness of Laser Welded Joints in the Ductile-Brittle Transition." *Eng. Fract. Mech.*, vol. 74, no. 15, pp. 2395–2419, 2007.

[12] E. Charalampopoulou, K. Lambrinou, T. Van der Donck, B. Paladino, F. Di Fonzo, C. Azina, P. Eklund, S. Mráz, J. M. Schneider, D. Schryvers, R. Delville. "Early Stages of Dissolution Corrosion in 316L and DIN 1.4970 Austenitic Stainless Steels With and Without Anticorrosion Coatings in Static Liquid Lead-Bismuth Eutectic (LBE) at 500 °C." *Mater. Charact.*, vol. 178, p. 111234, 2021.

[13] J. Kalivodová, D. Baxter, M. Schütze, and V. Rohr. "Corrosion Behaviour of Boiler Steels, Coatings and Welds in Flue Gas Environments." *Mater. Corros.*, vol. 59, no. 5, pp. 367–373, 2008.

[14] S. H. Cho, J. S. Cha, S. H. Kim, E. Y. Choi, J. H. Lee, and J. M. Hur. "Hot Corrosion Behaviour of Inconel 625 Weldments in Molten Lithium Salt." *Corros. Eng. Sci. Technol.*, vol. 50, no. 8, pp. 606–617, 2015.

[15] L. C. Olson, J. W. Ambrosek, K. Sridharan, M. H. Anderson, and T. R. Allen. "Materials Corrosion in Molten LiF–NaF–KF salt." *J. Fluor. Chem.*, vol. 130, no. 1, pp. 67–73, 2009.

[16] G. Le Petit, G. Douysset, G. Ducros, P. Gross, P. Achim, M. Monfort, P. Raymond, Y. Pontillon, C. Jutier, X. Blanchard, T. Taffary, and C. Moulin. "Analysis of Radionuclide Releases from the Fukushima Dai-Ichi Nuclear Power Plant Accident Part I." *Pure Appl. Geophys.*, vol. 171, no. 3–5, pp. 629–644, 2014.

[17] S. Lee and Y. Son, "A study on weld residual stress relaxation by local post weld heat treatment for circumferential weld," in *Volume 1: Plant Operations, Maintenance, Engineering, Modifications, Life Cycle and Balance of Plant; Nuclear Fuel and Materials; Plant Systems, Structures and Components; Codes, Standards, Licensing and Regulatory Issues*, Jul. 2014, pp. 1–7.

[18] Hyundai Welding, "SM-70 GAS METAL ARC WELDING CONSUMABLES FOR WELDING OF Mild & 490Mpa CLASS HIGH TENSILE STEEL," 2021. [Online]. Available: https://www.hyundaiwelding.com/data/file/consumables/ttr/SM-70.pdf

[19] C. Schroer and J. Konys. *Physical Chemistry of Corrosion and Oxygen Control in Liquid Lead and Lead-Bismuth Eutectic*, FZKA 7364, 2007.

[20] C. Fazio, G. Benamati, C. Martini, and G. Palombarini. "Compatibility Tests on Steels in Molten Lead and Lead-Bismuth," *J. Nucl. Mater.*, vol. 296, no. 1–3, pp. 243–248, 2001.

[21] K. Lambrinou, E. Charalampopoulou, T. Van der Donck, R. Delville, and D. Schryvers. "Dissolution corrosion of 316L austenitic stainless steels in contact with static liquid lead-bismuth eutectic (LBE) at 500 °C." *J. Nucl. Mater.*, vol. 490, no. 2017, pp. 9–27, 2017.

[22] J. Jiang, Y. Wang, and H. V. Atkinson. "Microstructural Coarsening of 7005 Aluminum Alloy Semisolid Billets with High Solid Fraction." *Mater. Charact.*, vol. 90, pp. 52–61, 2014.

[23] R. S. Coelho, A. Kostka, H. Pinto, S. Riekehr, M. Koçak, and A. R. Pyzalla. "Microstructure and Mechanical Properties of Magnesium Alloy AZ31B Laser Beam Welds." *Mater. Sci. Eng. A*, vol. 485, no. 1–2, pp. 20–30, 2008.